ISSN:1575-6807
D.L.: GC-1317-1999

INSTITUTO UNIVERSITARIO DE CIENCIAS Y TECNOLOGIAS CIBERNETICAS

Optical Flow Estimation with Large Displacements: A Temporal Regularizer

Agustin Salgado, Javier Sánchez.

Nº 0033

April 2006

Cuadernos del Instituto Universitario de Ciencias y Tecnologías Cibernéticas
Instituto Universitario de Ciencias y Tecnologías Cibernéticas
Universidad de Las Palmas de Gran Canaria
Campus de Tafira
35017 Las Palmas, España
http://www.iuctc.ulpgc.es

Optical Flow Estimation with Large Displacements: A Temporal Regularizer

A. Salgado and J. Sánchez
Computer Science Department,
University of Las Palmas de G. C.
Spain

Abstract

The aim of this work is to propose a model for computing the optical flow in a sequence of images with a spatio–temporal regularizer explicitly designed for large displacements. We study the introduction of a temporal regularizer that expands the information beyond two consecutive frames. We propose to decouple the spatial and temporal regularizing terms to avoid an incongruous formulation between the data and smoothness term. We use the large optical flow constraint equation in the data term, the Nagel–Enkelmann operator for the spatial smoothness term and a newly designed temporal regularization. Our model is based on an energy functional that yields a partial differential equation (PDE). This PDE is embedded into a multipyramidal strategy to recover large displacements. A gradient descent technique is applied at each scale to reach the minimum. The numerical experiments show that thanks to this regularizer the results are more stable and accurate.

1 Introduction

In this paper we consider the problem of estimating the optical flow assuming that the objects may undergo large displacements. The difference with respect to other related approaches is that we exploit the temporal dimension of the sequence. Most of the better known methods only deal with the problem of estimating the optical flow between two frames, ignoring that the sequence comprises several images which are all related. We show in this paper that it is possible to integrate the temporal information to improve the results and provide more stable solutions.

We propose a variational technique in where an energy functional is minimized yielding a diffusion–reaction PDE. These kind of energy–based approaches have been largely used in optical flow estimation. Horn and Schunck [14], for instance, propose to minimize the so–called optical flow constraint equation (OFC) together with a smoothing term depending on the optical flow gradient. Later some authors have proposed several improvements to overcome the shortcomings of this method like in [4], [9], [18], [10].

In order to compute large displacements a common strategy is to use a multi–pyramidal decomposition like in [4], [11] and [16] in where each scale is represented by decreasing size of images. A different approach is that of Alvarez et al. [3] that uses a linear scale–space approach in the focusing strategy. The idea behind all these methods is the same: use coarsest scales to compute raw estimates of the optical flow and utilize this as an approximation to finer scales. In a recent paper by Brox et al. [8] the authors state that the latter and former approaches are equivalent.

The first works on spatio–temporal methods are due to Nagel [17] and Black and Anandan [5]. The former propose an extension of his oriented smoothness operator by including the temporal dimension. The latter propose to compute the motion incrementaly assuming an acceleration in time. In order to make this method more robust to noise, the acceleration is averaged in time. More recently Weickert and Schnörr [23] propose a continuous model with a nonlinear convex spatio–temporal smoothness constraint. The spatial and temporal derivatives are formulated in a homogeneous way. Other related paper is due to Brox et al. [8]. In this case a Total Variation functional is used in the data and smoothing terms. The data term includes the large optical flow constraint equation and a gradient constancy term. The smoothness term is formulated continuously with spatial and temporal derivatives treated in the same manner.

In this work we propose a novel temporal regularizing term which is explicitly designed to support for large displacements. The previous mentioned spatio–temporal methods treat the spatial and temporal dimensions in the same way. We show here that when large displacements are present, it is not suitable to use temporal derivatives. It is more convenient to separate the temporal smoothing term. We also show that the major contributions of spatio–temporal smoothness are given by more stable and accurate results. This is clearly stated in the experimental results in where some comparisons with its corresponding spatial method is carried out on synthetic and real sequences.

In Sect. 2 we give an overview on related optical flow methods and a study on the generalization of spatial optical flows. In Sect. 2.1 we introduce and justify the use of temporal regularizers. In Sect. 3 we derive the numerical scheme for the energy proposed in the previous section and in Sect. 5 we demonstrate the performance of our method by using synthetic and real sequences and compare with spatial methods. Finally in Sect. 6 the conclusions.

2 The Method

The optical flow, $\mathbf{h}(\mathbf{x}) = (u(\mathbf{x}), v(\mathbf{x}))^T$, is the apparent motion of pixels in a sequence of images. One of the first in introducing a variational formulation for the computation of the optical flow was Horn and Schunck [14]. They proposed the so–called optical flow constraint equation

$$\frac{dI(\mathbf{x},t)}{dt} = \nabla I \cdot \mathbf{h} + I_t = 0 \tag{1}$$

which states that the image intensity remains constant through the sequence –known as the Lambertian assumption–. This was a natural way to come across with the estimation of the optical flow from a differential equation. They proposed to minimize the square of (1) together with the square norm of the optical flow gradient.

Ec. (1) is valid when the object displacements in the scene are continuous. This is not the case in our approach since the objects may undergo large displacements. A different formulation which is the corresponding to the optical flow constraint equation in the discontinuous case is

$$I_1(\mathbf{x}) - I_2(\mathbf{x} + \mathbf{h}(\mathbf{x})) = 0 \tag{2}$$

In fact, Ec. (1) is the Taylor expansion of (2) up to the first derivative, so the former is an approximation to the latter equation. Ec. (1) and (2) are very similar in spirit but the latter one only formulated for two frames. Extending Ec. (2) to consider all the frames and using a squared functional we obtain the minimizer

$$\sum_{i=1}^{N-1} \left(I_i(\mathbf{x}) - I_{i+1}(\mathbf{x} + \mathbf{h}_i(\mathbf{x}))\right)^2 \tag{3}$$

where N is the number of frames and i subindex stands for the temporal dimension.

Other approaches different from the quadratic form are commonly used, thus, in general, a data term will be a functional like

$$\sum_{i=1}^{N-1} \mathcal{D}\left(I_i(\mathbf{x}), I_{i+1}(\mathbf{x}), \mathbf{h}_i(\mathbf{x})\right) \tag{4}$$

where $\mathcal{D}(.)$ could be chosen depending on the nature of the images. For instance, in papers [6], [7], [15] the authors propose some robusts functionals instead of a quadratic form in order to decrease the effect of outliers. It also may be replaced by other non–Lambertian functionals in order to deal with more realistic image sequences. In paper [12] the authors proposed a method for dealing with varying brightness of the image intensities and more robust approaches are given in [22], [21] and [13], based on multimodal image matching to deal with complex image intensity transformations.

We may still generalize Ec. (4) if we assume that there could be any relation not only with consecutive frames but also with any two frames of the sequence. A more general data term is

$$\sum_{i=1}^{N} \sum_{j=1, j\neq i}^{N} \mathcal{D}\left(I_i(\mathbf{x}), I_j(\mathbf{x}), \mathbf{h}_{ij}(\mathbf{x})\right) \tag{5}$$

in where we may consider that there exists an optical flow function between any two frames – regard that in this case the forward and backward optical flows are introduced in a single formulation–. Ec. (5) puts in correspondence frames that could be very far and introduces an overload in the process due to the bigger amount of unknowns. This is interesting if we want to carry out a long–term analysis of the data. Our purpose here is to show the benefits

of introducing temporal regularizers for the estimation of optical flows, thus, in the following we will use Ec. (3) which is a special case of (5).

Typically, the data term is accompanied by a smoothness term depending on the gradient of the flow. Horn and Schunck [14], for instance, proposed to minimize the square norm of the optical flow gradient

$$\|\nabla \mathbf{h}\|^2 = \|\nabla u\|^2 + \|\nabla v\|^2 \tag{6}$$

which provides smooth solutions and yields an isotropic diffusion equation at the PDE. This model has been improved during the last years and some authors has introduced some different approaches in order to respect the image or flow discontinuities. A well–known approach is that of Nagel–Enkelmann [18] that introduce an operator depending on the image gradient that enables anisotropic diffusion in order to respect the object contours. Other improvements are given by the methods explained in [3], [9], [20] and [10]. In paper [24] the authors stablish a common framework to deal with different regularization terms ranging from flow driven to image driven and from isotropic to anisotropic smoothing and also study the existence and uniqueness of solutions.

Most of the above mentioned methods are designed for two frames. In our case we have to extend the problem to multiple images by introducing an addition as we did for the data term. In general, our regularizing term will depend on the optical flow gradient and also on the image gradient

$$\sum_{i=1}^{N-1} \mathcal{R}\left(\nabla I_i(\mathbf{x}), \nabla \mathbf{h}_i(\mathbf{x})\right) \tag{7}$$

We may still generalize Ec. (7) to consider optical flow functions like in (5) as

$$\sum_{i=1}^{N} \sum_{j=1, j\neq i}^{N} \mathcal{R}\left(\nabla I_i(\mathbf{x}), \nabla \mathbf{h}_{ij}(\mathbf{x})\right) \tag{8}$$

Regard that in this case we use a spatial gradient both for the images and for the optical flows. This means that the regularization is only carried out spatially –most of the methods explained so far use spatial regularizations–. In the following section we examine how to introduce a temporal regularizer.

To sum up, our spatial energy is as follows:

$$E(\mathbf{h}_1, \ldots, \mathbf{h}_{N-1}) = \sum_{i=1}^{N-1} \int_{\Omega} \mathcal{D}(I_i, I_{i+1}, \mathbf{h}_i)\, d\omega + \alpha \sum_{i=1}^{N-1} \int_{\Omega} \mathcal{R}(\nabla I_i, \nabla \mathbf{h}_i)\, d\omega \tag{9}$$

In the sequel we use the standard optical flow constraint equation for large displacements (3) in place of $\mathcal{D}(I_i, I_{i+1}, \mathbf{h}_i)$ and we choose the Nagel–Enkelmann operator for the smoothness term.

Following the generalizations of (5) and (7) a more general energy functional is

$$E(\mathbf{h}_{12},\ldots,\mathbf{h}_{N(N-1)}) = \sum_{i=1}^{N}\sum_{j=1,j\neq i}^{N}\int_{\Omega}\mathcal{D}(I_i,I_j,\mathbf{h}_{ij})\,d\omega + \alpha\sum_{i=1}^{N}\sum_{j=1,j\neq i}^{N}\int_{\Omega}\mathcal{R}(\nabla I_i,\nabla\mathbf{h}_{ij})\,d\omega \quad (10)$$

2.1 Introducing a temporal regularizer

Most of the methods on variational optical flow estimation use spatial regularizers to enable smooth solutions. Typically, the smoothness is restricted to two frames since there is no transfer of information beyond consecutive images. There is no way to obtain a global smooth solution when only spatial gradients are used. This shortcoming makes us think of the need of introducing a temporal regularizer that enables an overall smoothing of the optical flows.

Variational temporal regularizers have been introduced in some works like in [5] and [17]. More recently Weickert and Schnörr [23] introduced a method in where they used the continuous optical flow constraint equation (1) as data term and a regularizing term of the form $\mathcal{R}(|\nabla_3 u|^2+|\nabla_3 v|^2)$. In this case the temporal derivative is treated in the same manner as the spatial derivatives. This has the advantage of beeing an homogeneous formulation that does not make any difference between the spatial and temporal dimensions. The continuous formulation of this method restricts the scope of the method to images with small displacements of the objects.

In [8] a similar method is proposed. In this case they use a data term which is based on the large optical flow constraint equation (2) and as regularizing term they use a variation of the approach in [23] –$\mathcal{R}(|\nabla_3 u|^2+|\nabla_3 v|^2)$–. The former is thus designed to support for large displacements meanwhile the second is designed continuously which means that it only supports for short displacements.

This proposal has two major inconveniences: the first one is due to the fact that the temporal and spatial components of the gradient are coupled and when large displacements are present, the temporal estimate inhibits regularization on the spatial domain; The second inconvenience is due to the fact that the model uses a temporal derivative in the smoothness term, so it supposes a continuity of the flow in time but the data term allows discontinuities in time.

A simple way to overcome the first drawback is to replace $\mathcal{R}(|\nabla_3 u|^2+|\nabla_3 v|^2)$ with separate spatial and temporal regularizers as $\mathcal{R}(|\nabla u|^2+|\nabla v|^2)+\mathcal{T}(|u_t|^2+|v_t|^2)$, but still the temporal term is formulated continuously. If we also want to deal with large displacements, then it is necessary to replace the temporal derivative with a different estimate.

Let us know consider what kind of estimates we might use in $\mathcal{T}(.)$. If $\mathbf{h}(\mathbf{x})$ is large at a given point $\mathbf{x}$ then it does not make sense to compute $\mathbf{h}_t=(u_t,v_t)^T$, since it will not be continuous. If we suppose that the object velocities are smooth in the sequence, then we know that given two consecutive frames the value of the optical flow, $\mathbf{h}_i(\mathbf{x})$, for a given

frame should be similar to the optical flow in the following frame at the position given by $\mathbf{h}_{i+1}(\mathbf{x}+\mathbf{h}_i(\mathbf{x}))$. Our estimate should be a functional of the form $\mathcal{T}(\mathbf{h}_i(\mathbf{x}), \mathbf{h}_{i+1}(\mathbf{x}+\mathbf{h}_i(\mathbf{x})))$.

We propose the following energy

$$\begin{aligned} E(\mathbf{h}) &= \sum_{i=1}^{N-1} \int_{\Omega} \mathcal{D}(I_i, I_{i+1}, \mathbf{h}_i)\ d\omega \\ &\quad +\alpha \sum_{i=1}^{N-1} \int_{\Omega} \mathcal{R}(\nabla I_i, \nabla \mathbf{h}_i)\ d\omega \\ &\quad +\beta \sum_{i=1}^{N-1} \int_{\Omega} \mathcal{T}(\mathbf{h}_i, \mathbf{h}_{i+1})\ d\omega \end{aligned} \tag{11}$$

As we mentioned before we use the large optical flow constraint equation (3) for $\mathcal{D}(.)$, the Nagel–Enkelmann operator for $\mathcal{R}(.)$ and $T(\mathbf{h}_i, \mathbf{h}_{i+1}) = \Phi(\|\mathbf{h}_i - \mathbf{h}_{i+1}(\mathbf{x}+\mathbf{h}_i)\|^2)$

$$\begin{aligned} E(\mathbf{h}) &= \sum_{i=1}^{N-1} \int_{\Omega} \left(I_i - I_{i+1}\left(\mathbf{x}+\mathbf{h}_i\right)\right)^2\ d\omega \\ &\quad +\alpha \sum_{i=1}^{N-1} \int_{\Omega} trace(\nabla \mathbf{h}_i^T \mathbf{D}(\nabla I_i) \nabla \mathbf{h}_i^T)\ d\omega \\ &\quad +\beta \sum_{i=1}^{N-2} \int_{\Omega} \Phi(\|\mathbf{h}_i - \mathbf{h}_{i+1}(\mathbf{x}+\mathbf{h}_i)\|^2)\ d\omega \end{aligned} \tag{12}$$

where $\Phi(x^2) = 1 - \gamma e^{-\frac{x^2}{\gamma}}$. This is the same as saying that the optical flows remain constant all through the sequence. When displacements are very small, $\mathbf{h}_i - \mathbf{h}_{i+1}(\mathbf{x}+\mathbf{h}_i)$ is an approximation of the temporal derivative. This kind of estimate will favour translational with constant velocities.

One inconvenience of the previous approach is that there is only transfer of information from the last optical flows towards the early ones. One way to compensate for this is to turn the method symmetrical by including the backward optical flows, $\mathbf{h}^*$ (see appendix A), as

$$
\begin{aligned}
E(\mathbf{h}) &= \sum_{i=1}^{N-1} \int_{\Omega} \left(I_i - I_{i+1}\left(\mathbf{x}+\mathbf{h}_i\right)\right)^2 \, d\omega \\
&+\alpha \sum_{i=1}^{N-1} \int_{\Omega} trace(\nabla \mathbf{h}_i^T \mathbf{D}(\nabla I_i) \nabla \mathbf{h}_i^T) \, d\omega \\
&+\beta \sum_{i=1}^{N-2} \int_{\Omega} \Phi(\|\mathbf{h}_i - \mathbf{h}_{i+1}(\mathbf{x}+\mathbf{h}_i)\|^2) \, d\omega \\
&+\beta \sum_{i=2}^{N-1} \int_{\Omega} \Phi(\left\|\mathbf{h}_i - \mathbf{h}_{i-1}(\mathbf{x}+\mathbf{h}^*_{i-1})\right\|^2) \, d\omega
\end{aligned} \tag{13}
$$

With the last two integrals we are implicitly assuming a model for the object velocities. We enforce that the $\mathbf{h}_i$ functions be similar in magnitude and direction, so this scheme is more suitable for objects that move with constant velocity in a permanent direction. When it moves away from this model, function $\Phi(.)$ will decrease the effect of $\mathcal{T}(.)$ and the temporal regularization will be useless.

It is difficult to find a simple model for $\mathcal{T}(.)$ that takes into account all the possible configurations of velocities of a real sequence. Different alternatives of the temporal term may be given by different functionals like $\Phi(\|\mathbf{h}_i\|^2 - \|\mathbf{h}_{i+1}(\mathbf{x}+\mathbf{h}_i)\|^2) + \Phi(\|\mathbf{h}_i\|^2 - \left\|\mathbf{h}_{i-i}(\mathbf{x}+\mathbf{h}^*_{i-1})\right\|^2)$ in where we minimize the difference between the magnitude of the optical flows, which could favour constant velocities estimation independently of whether they rotate or traslate. In any case, we are assuming a displacement pattern that will favour some kind of movements opposed to others.

3 Minimizing the Energy

In order to obtain a solution to our energy we derive the Euler–Lagrange equations:

$$
\begin{aligned}
\mathbf{0} &= -\left(I_i(\mathbf{x}) - I_{i+1}(\mathbf{x}+\mathbf{h}_i)\right) \nabla I_{i+1}(\mathbf{x}+\mathbf{h}_i) \\
&-\alpha \, \left(\mathbf{div}(\mathbf{D}\left(\nabla \mathbf{h}_i\right)\nabla u_i), \mathbf{div}(\mathbf{D}\left(\nabla \mathbf{h}_i\right)\nabla v_i)\right)^T \\
&+\beta \, \Phi'(\|\mathbf{h}_i - \mathbf{h}_{i+1}(\mathbf{x}+\mathbf{h}_i)\|^2) \\
&\cdot \Big(\left(\mathbf{h}_i - \mathbf{h}_{i+1}(\mathbf{x}+\mathbf{h}_i)\right)^T \left(\mathbf{Id} - \nabla \mathbf{h}^T_{i+1}(\mathbf{x}+\mathbf{h}_i)\right) \Big) \\
&+\beta \Phi'(\left\|\mathbf{h}_i - \mathbf{h}_{i-1}(\mathbf{x}+\mathbf{h}^*_{i-1})\right\|^2) \\
&\cdot \left(\mathbf{h}_i - \mathbf{h}_{i-1}(\mathbf{x}+\mathbf{h}^*_{i-1})\right)
\end{aligned} \tag{14}
$$

We apply a gradient descent technique to reach the solution of the previous system of equations:

$$
\begin{aligned}
\frac{\partial \mathbf{h}_i}{\partial t} &= (I_i(\mathbf{x}) - I_{i+1}(\mathbf{x}+\mathbf{h}_i))\,\frac{\partial I_{i+1}(\mathbf{x}+\mathbf{h}_i)}{\partial x} \\
&\quad +\alpha\ (\mathbf{div}(\mathbf{D}\,(\nabla \mathbf{h}_i)\,\nabla u_i), \mathbf{div}(\mathbf{D}\,(\nabla \mathbf{h}_i)\,\nabla v_i))^T \\
&\quad -\beta\,\Phi'(\|\mathbf{h}_i - \mathbf{h}_{i+1}(\mathbf{x}+\mathbf{h}_i)\|^2) \\
&\quad \cdot \Big((\mathbf{h}_i - \mathbf{h}_{i+1}(\mathbf{x}+\mathbf{h}_i))^T \left(\mathbf{Id} - \nabla \mathbf{h}_{i+1}^T(\mathbf{x}+\mathbf{h}_i)\right)\Big) \\
&\quad -\beta\,\Phi'(\left\|\mathbf{h}_i - \mathbf{h}_{i-1}(\mathbf{x}+\mathbf{h}_{i-1}^*)\right\|^2) \\
&\quad \cdot \left(\mathbf{h}_i - \mathbf{h}_{i-1}(\mathbf{x}+\mathbf{h}_{i-1}^*)\right)
\end{aligned} \tag{15}
$$

where $i = 1, \ldots N-1$, thus we have a system of $N-1$ pair of equations correponding to the optical flows of the complete sequence.

We embed this gradient descent equations into a multi–pyramidal approach to deal with large displacements. This is a coarse–to–fine strategy commonly used in other works on optical flow estimation like in [4], [11], [8] and [16]. We create a pyramid of scales for the whole sequence with different size of images and solve the previous system of equations at each level. Once we obtain a stable solution for a scale we use this as a first estimate for a finer scale.

Therefore we have a number of scales $s_1, s_2, \ldots s_n$ each one representing different size of images. Normally the pyramid is formed by half sized images – the ratio between two images is 0,5 – but other ratios may be considered like in [8] where they propose to use a reduction factor η between 0,5 and 0,95. At each scale we solve the previous system of equations for the whole set of unknows $\{u_i^s, v_i^s\}$ and then we use this as a first approximation for the following scale $\{u_i^{s_1}, v_i^{s_1}\} \rightarrow \{u_i^{s_2}, v_i^{s_2}\} \rightarrow \ldots \{u_i^{s_n}, v_i^{s_n}\}$.

4 Numerical scheme

In this section we describe an implicit numerical scheme to solve the system of equations given by (15). We use finite differences to approximate the spatial derivatives. Using the following notation for the components of matrix $\mathbf{D}\,(\nabla I_{i,j,k}) = \begin{pmatrix} a & b \\ b & c \end{pmatrix}$ our numerical approximation is given by

$$
\begin{aligned}
\frac{u_{i,j,k}^{n+1}-u_{i,j,k}^{n}}{\tau} &= \left(I_{i,j,k}-I_{i,j,k+1}^{\mathbf{h}_{i,j,k}^{n}}+u_{i,j,k}^{n+1}I_{x_{i,j,k+1}}^{\mathbf{h}_{i,j,k}^{n}}+v_{i,j,k}^{n+1}I_{y_{i,j,k+1}}^{\mathbf{h}_{i,j,k}^{n}}\right)I_{x_{i,j,k+1}}^{\mathbf{h}_{i,j,k}^{n}}\\
&-u_{i,j,k}^{n+1}I_{x_{i,j,k+1}}^{2,\mathbf{h}_{i,j,k}^{n}}-v_{i,j,k}^{n+1}I_{y_{i,j,k+1}}^{\mathbf{h}_{i,j,k}^{n}}I_{x_{i,j,k+1}}^{\mathbf{h}_{i,j,k}^{n}}\\
&+\alpha\left(\frac{a_{i+1,j,k}+a_{i,j}}{2}\frac{u_{i+1,j,k}^{n+1}-u_{i,j,k}^{n}}{h_1^2}+\frac{a_{i-1,j,k}+a_{i,j}}{2}\frac{u_{i-1,j,k}^{n+1}-u_{i,j,k}^{n+1}}{h_1^2}\right.\\
&+\frac{c_{i,j+1,k}+c_{i,j}}{2}\frac{u_{i,j+1,k}^{n+1}-u_{i,j,k}^{n+1}}{h_2^2}+\frac{c_{i,j-1,k}+c_{i,j}}{2}\frac{u_{i,j-1,k}^{n+1}-u_{i,j,k}^{n+1}}{h_2^2}\\
&+\frac{b_{i+1,j+1,k}+b_{i,j}}{2}\frac{u_{i+1,j+1,k}^{n+1}-u_{i,j,k}^{n+1}}{2h_1h_2}+\frac{b_{i-1,j-1,k}+b_{i,j}}{2}\frac{u_{i-1,j-1,k}^{n+1}-u_{i,j,k}^{n+1}}{2h_1h_2}\\
&\left.+\frac{b_{i+1,j-1,k}+b_{i,j}}{2}\frac{u_{i+1,j-1,k}^{n+1}-u_{i,j,k}^{n+1}}{2h_1h_2}+\frac{b_{i-1,j+1,k}+b_{i,j}}{2}\frac{u_{i-1,j+1,k}^{n+1}-u_{i,j,k}^{n+1}}{2h_1h_2}\right)\\
&-\beta\Phi'\left[\left(u_{i,j,k}^{n+1}-u_{i,j,k+1}^{n,\mathbf{h}_{i,j,k}^{n}}+u_{i,j,k}^{n+1}u_{x_{i,j,k+1}}^{n,\mathbf{h}_{i,j,k}^{n}}+v_{i,j,k}^{n+1}u_{y_{i,j,k+1}}^{n,\mathbf{h}_{i,j,k}^{n}}\right)\left(1-u_{x_{i,j,k+1}}^{n,\mathbf{h}_{i,j,k}^{n}}\right)\right.\\
&-u_{i,j,k}^{n+1}u_{x_{i,j,k+1}}^{n,\mathbf{h}_{i,j,k}^{n}}\left(1-u_{x_{i,j,k+1}}^{n,\mathbf{h}_{i,j,k}^{n}}\right)-v_{i,j,k}^{n+1}u_{y_{i,j,k+1}}^{n,\mathbf{h}_{i,j,k}^{n}}\left(1-u_{x_{i,j,k+1}}^{n,\mathbf{h}_{i,j,k}^{n}}\right)\\
&+\left(v_{i,j,k}^{n+1}-v_{i,j,k+1}^{n,\mathbf{h}_{i,j,k}^{n}}+u_{i,j,k}^{n+1}v_{x_{i,j,k+1}}^{n,\mathbf{h}_{i,j,k}^{n}}+v_{i,j,k}^{n+1}v_{y_{i,j,k+1}}^{n,\mathbf{h}_{i,j,k}^{n}}\right)v_{x_{i,j,k+1}}^{n,\mathbf{h}_{i,j,k}^{n}}\\
&\left.-u_{i,j,k}^{n+1}v_{x_{i,j,k+1}}^{2,n,\mathbf{h}_{i,j,k}^{n}}-v_{i,j,k}^{n+1}v_{y_{i,j,k+1}}^{n,\mathbf{h}_{i,j,k}^{n}}v_{x_{i,j,k+1}}^{n,\mathbf{h}_{i,j,k}^{n}}\right]\\
&-\beta\Phi'\left[u_{i,j,k}^{n+1}-u_{i,j,k+1}^{n,\mathbf{h}_{i,j,k}^{*,n}}\right] \qquad (16)
\end{aligned}
$$

$$
\begin{aligned}
\frac{v_{i,j,k}^{n+1}-v_{i,j,k}^{n}}{\tau} &= \left(I_{i,j,k}-I_{i,j,k+1}^{\mathbf{h}_{i,j,k}^{n}}+u_{i,j,k}^{n+1}I_{x_{i,j,k+1}}^{\mathbf{h}_{i,j,k}^{n}}+v_{i,j,k}^{n+1}I_{y_{i,j,k+1}}^{\mathbf{h}_{i,j,k}^{n}}\right)I_{y_{i,j,k+1}}^{\mathbf{h}_{i,j,k}^{n}}\\
&-u_{i,j,k}^{n+1}I_{x_{i,j,k+1}}^{\mathbf{h}_{i,j,k}^{n}}I_{y_{i,j,k+1}}^{\mathbf{h}_{i,j,k}^{n}}-v_{i,j,k}^{n+1}I_{y_{i,j,k+1}}^{2,\mathbf{h}_{i,j,k}^{n}}\\
&+\alpha\left(\frac{a_{i+1,j,k}+a_{i,j}}{2}\frac{v_{i+1,j,k}^{n+1}-v_{i,j,k}^{n+1}}{h_1^2}+\frac{a_{i-1,j,k}+a_{i,j}}{2}\frac{v_{i-1,j,k}^{n+1}-v_{i,j,k}^{n+1}}{h_1^2}\right.\\
&+\frac{c_{i,j+1,k}+c_{i,j}}{2}\frac{v_{i,j+1,k}^{n+1}-v_{i,j,k}^{n+1}}{h_2^2}+\frac{c_{i,j-1,k}+c_{i,j}}{2}\frac{v_{i,j-1,k}^{n+1}-v_{i,j,k}^{n+1}}{h_2^2}\\
&+\frac{b_{i+1,j+1,k}+b_{i,j}}{2}\frac{v_{i+1,j+1,k}^{n+1}-v_{i,j,k}^{n+1}}{2h_1h_2}+\frac{b_{i-1,j-1,k}+b_{i,j}}{2}\frac{v_{i-1,j-1,k}^{n+1}-v_{i,j,k}^{n+1}}{2h_1h_2}\\
&\left.+\frac{b_{i+1,j-1,k}+b_{i,j}}{2}\frac{v_{i+1,j-1,k}^{n+1}-v_{i,j,k}^{n+1}}{2h_1h_2}+\frac{b_{i-1,j+1,k}+b_{i,j}}{2}\frac{v_{i-1,j+1,k}^{n+1}-v_{i,j,k}^{n+1}}{2h_1h_2}\right)\\
&-\beta\Phi'\left[\left(v_{i,j,k}^{n+1}-v_{i,j,k+1}^{n,\mathbf{h}_{i,j,k}^{n}}+u_{i,j,k}^{n+1}v_{x_{i,j,k+1}}^{n,\mathbf{h}_{i,j,k}^{n}}+v_{i,j,k}^{n+1}v_{y_{i,j,k+1}}^{n,\mathbf{h}_{i,j,k}^{n}}\right)\left(1-v_{y_{i,j,k+1}}^{n,\mathbf{h}_{i,j,k}^{n}}\right)\right.\\
&-u_{i,j,k}^{n+1}v_{x_{i,j,k+1}}^{n,\mathbf{h}_{i,j,k}^{n}}\left(1-v_{y_{i,j,k+1}}^{n,\mathbf{h}_{i,j,k}^{n}}\right)-v_{i,j,k}^{n+1}v_{y_{i,j,k+1}}^{n,\mathbf{h}_{i,j,k}^{n}}\left(1-v_{y_{i,j,k+1}}^{n,\mathbf{h}_{i,j,k}^{n}}\right)\\
&+\left(u_{i,j,k}^{n+1}-u_{i,j,k+1}^{n,\mathbf{h}_{i,j,k}^{n}}+u_{i,j,k}^{n+1}u_{x_{i,j,k+1}}^{n,\mathbf{h}_{i,j,k}^{n}}+v_{i,j,k}^{n+1}u_{y_{i,j,k+1}}^{n,\mathbf{h}_{i,j,k}^{n}}\right)u_{y_{i,j,k+1}}^{n,\mathbf{h}_{i,j,k}^{n}}\\
&\left.-u_{i,j,k}^{n+1}u_{x_{i,j,k+1}}^{n,\mathbf{h}_{i,j,k}^{n}}u_{y_{i,j,k+1}}^{n,\mathbf{h}_{i,j,k}^{n}}-v_{i,j,k}^{n+1}u_{y_{i,j,k+1}}^{2,n,\mathbf{h}_{i,j,k}^{n}}\right]\\
&-\beta\Phi'\left[v_{i,j,k}^{n+1}-v_{i,j,k+1}^{n,\mathbf{h}_{i,j,k}^{*,n}}\right] \qquad (17)
\end{aligned}
$$

where j,k stands for the pixel location and $I_{i+1,j,k}^{\mathbf{h}_{i,j,k}^{n+1}}=I_{i+1}(\mathbf{x}_{j,k}+\mathbf{h}_{i,j,k}^{n+1})$. Subindex i still represents the temporal dimension,τ is the time step which is always fixed in the experimental results to 10 and $v_{y_{i,j,k+1}}$ represents the y derivative of v at frame i in pixel $(j,k+1)$ also approximated with finite differences.

We solve the previous linear system (16) and (17) iteratively by a Gauss–Seidel algorithm.

5 Experimental Results

The purpose of these experimental results is to show the performance of our novel method with respect to its spatial counterpart. We are also interested in comparing this new method with its simple form given by the forward temporal cost matching function $\mathcal{T}(x)=\Phi(\|\mathbf{h}_i-\mathbf{h}_{i+1}(+\mathbf{h}_i)\|^2)$. In the sequel we name the spatial method – Eq. (9) – as "Spatial", the simpler temporal method as "Temporal" and the complete temporal method as "Bi–Temporal" or "Bidirectional–Temporal" – Eq. (13) –.

5.1 Translating square

The first sequence consists of ten frames with a black square moving ten pixels horizontally forward with a constant velocity over a white background. In Fig. 1 we can see several frames of the sequence. In Fig. 2 and 3 we show the euclidean and angular errors for all the frames using the three methods. In table 1 we show the mean angular and euclidean errors.

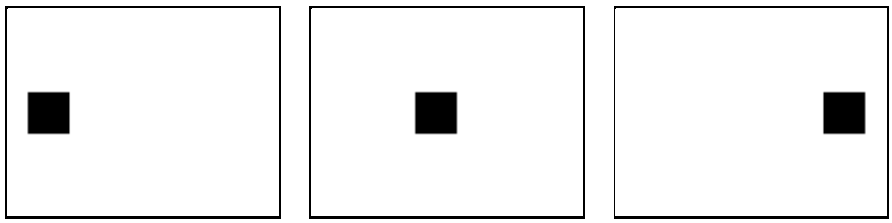

Figure 1: Frames 0, 4 and 9 of the square sequence.

From table 1 and Fig. 2 and 3 we can see that the temporal methods are very stable: the euclidean and angular errors for all the frames are very similar. However, the "Spatial" method is clearly unstable.

The improvement of the "Temporal" method with respect to its spatial counterpart is about 13,79% of the angular error and in the case of the "Bi–Temporal" is about 24,14%. The euclidean error for the "Temporal" method is bigger than the spatial method. This is justifiable because the last optical flow has a big error with respect to the rest of frames. The simple temporal method does not improve the last solution because it does not receive information from other frames. Even more, when this last estimate is bad, it propagates the bad guests to the rest of sequence. In the case of the "Bi–Temporal" method the improvement with respect to the spatial one is about 31,58%. This method is not affected by the last optical flow as in the previous case.

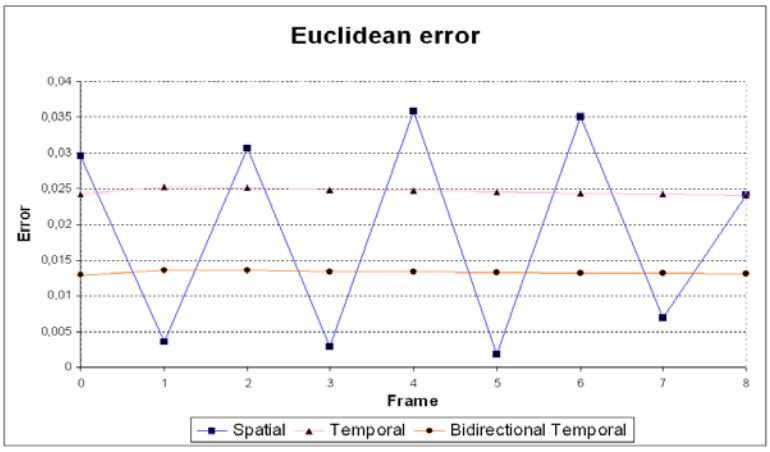

Figure 2: Euclidean error for the square sequence.

The performance of the temporal methods is much better than the spatial method. In this test, the optical flow is constant in magnitude and orientation. This kind of displacements

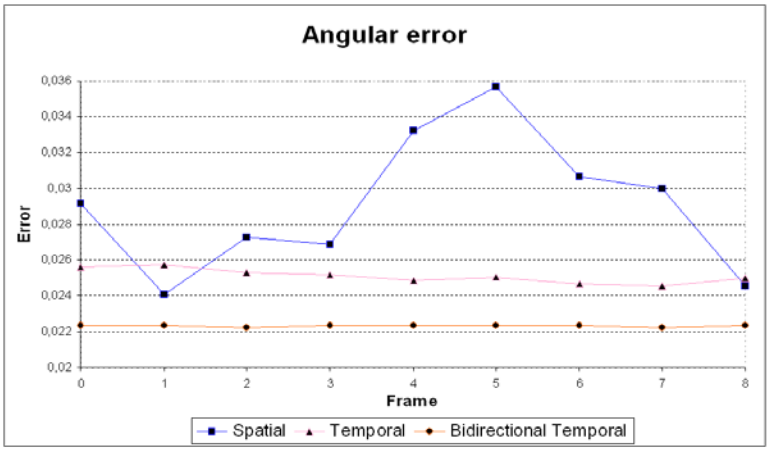

Figure 3: Angular error for the square sequence.

Method	AE_μ	AE_σ	EE_μ	EE_σ
Spatial	$0{,}029^o$	$3{,}6E\text{-}3^o$	0,0189	0,013
Temporal	$0{,}025^o$	$3{,}7E\text{-}4^o$	0,0246	3,8E-4
Bi-Temporal	$0{,}022^o$	$3{,}0E\text{-}5^o$	0,0132	1,9E-4

Table 1: Mean angular and euclidean errors for the square sequence: AE_μ is the mean angular error and AE_σ its standard deviation; EE_μ is the mean euclidean error and EE_σ its standard deviation.

can be estimated with high accuracy using our temporal term. Thus our method is very suitable for objects displacing with constant velocity through a given direction.

5.2 Marble Blocks

We used the Marble Block sequence – Fig. 4 – for the second test. This sequence is composed of 30 frames and is copyright by H.-H. Nagel (KOGS/IAKS, University of Karlsruhe, Germany, at *http://i21www.ira.uka.de/image_sequences/*.

Figure 4: Frames 0, 10 and 20 of the Marble Blocks sequence.

In Fig. 5 we can see the ground truth and the flows obtained with the spatial and

temporal methods.

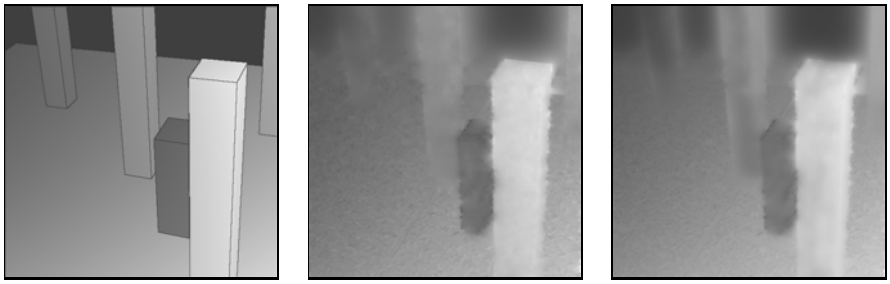

Figure 5: On the left, the true disparity associated with frame 10; in the middle, the optical flow corresponding to the spatial method; and, on the right, the solution for the bidirectional temporal method.

If we look at this image we observe that both solutions are similar but there are some differences: The floor is smoother in the temporal disparity map and the background is more respected. The right tower that disappears seems more continuous but, on the other hand, in the middle of the two left–most towers the disparity maps seem under–estimated. Globally, the temporal method seems to have better estimated the object discontinuities and the results inside each object are smoother.

In Figs. 6 and 7 we show the euclidean and angular errors for every frame of the sequence – for convenience we only show the central frames –. In both cases the spatial method provides worse and less stable results. Nearly all the results for the temporal methods are improved. In all cases, the "Bi-Temporal" performs in a similar way as the "Temporal" but with a smaller magnitude.

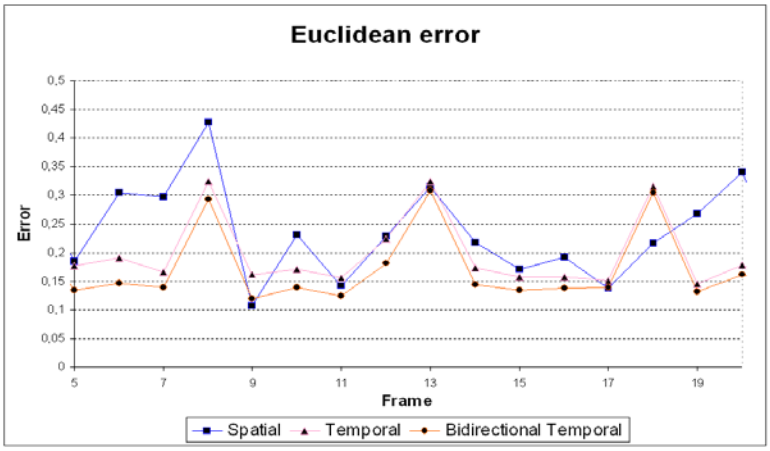

Figure 6: Euclidean error for the Marble Block sequence.

As we could expect, the results obtained for this sequence are improved. This sequence is similar to the translating square in the sense that the objects are moving with constant velocity in the same direction. In fact, the average motion of the sequence is 1,33 – with

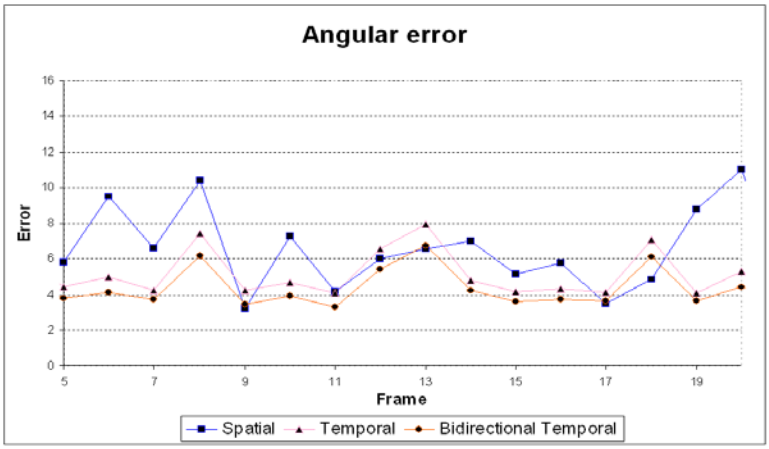

Figure 7: Angular error for the Marble Block sequence.

standard deviation 0,03 – except for frames 4, 8, 13, 18, 23 and 28 in which the average motion is 1,58 – with standard deviation 0,02–. This means that there is a shift on the magnitude of the velocities at these frames. If we look at these frames in Figs.6 and 7 we observe maximum peaks that reduce the stability of the temporal methods. We suppose that this sequence was captured with different frame rates at these particular frames.

Method	AE_μ	AE_σ	EE_μ	EE_σ
Spatial	$6{,}695^o$	$2{,}698^o$	0,2480	0,0963
Temporal	$5{,}402^o$	$1{,}327^o$	0,2081	0,0638
Bi-Temporal	$4{,}731^o$	$1{,}330^o$	0,1848	0,0661

Table 2: Mean angular and euclidean errors for the Marble Block sequence.

In table 2 we show the angular and euclidean errors and their standard deviations. The improvement of the "Temporal" method with respect to the "Spatial" one is about 19,31% for the angular error and 12,05% for the euclidean error. The improvement of the "Bi-Temporal" is about 29,33% for the angular and 25,48% for the euclidean error. In both cases the standard deviations are considerably reduced in a similar magnitude.

5.3 Yosemite

For the last synthetic test we used the Yosemite sequence – Fig. 8 –. This sequence was created by Lynn Quam and is available at *ftp://ftp.csd.uwo.ca/pub/vision*. A simpler version without clouds is available at *http://www.cs.brown.edu/people/ black/images.html*.

It combines both divergent and translational motions. The scene simulates a plane travel over the Yosemite mountains. The divergent motion is predominant. Motions in the center of the scene are nearly zero and there are different velocities and accelerations. This kind of displacements are not suitable for our model but we are interested on the study of the behaviour of our model with different configurations.

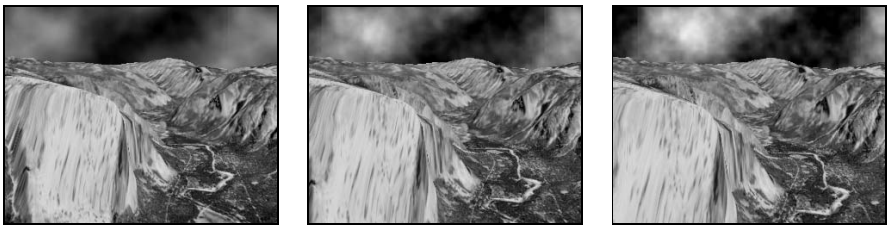

Figure 8: Frames 0, 7 and 14 of the Yosemite sequence.

In Fig. 9 we show the true disparity map and that provided by the spatial and bidirectional temporal methods. The differences of the last two are not appreciable, but if we look at the euclidean and angular errors – Figs. 10 and 11 – we may obtain some conclusions.

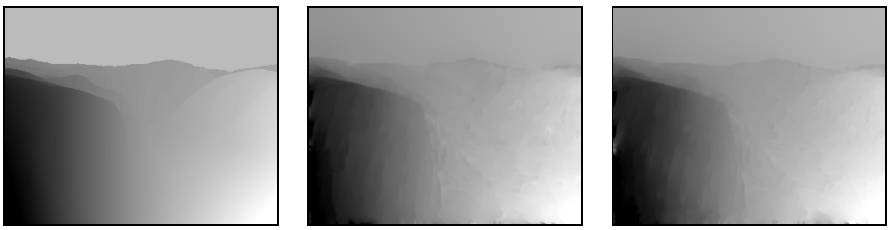

Figure 9: On the left, the true disparity map; in the middle, the result of the spatial method; and, on the right, the disparity map obtained with the bidirectional temporal method.

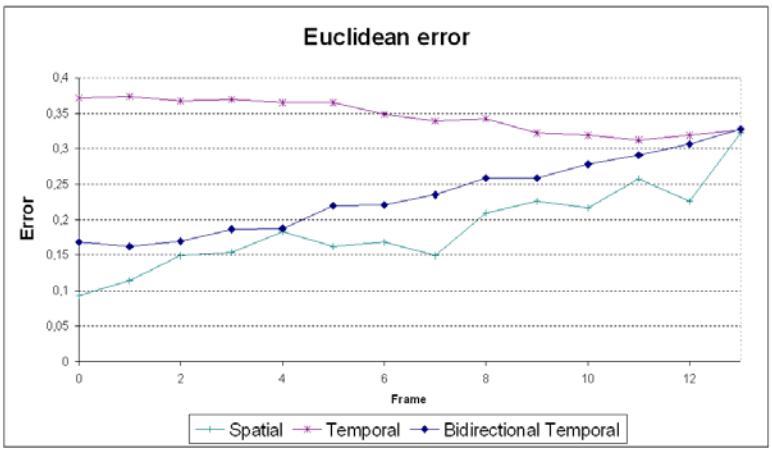

Figure 10: Euclidean error for the Yosemite sequence.

As we could expect, in both cases the errors due to the temporal methods are bigger. The simple temporal method propagates the bad results from the last frame to the previous ones, so the error increases backwards. The bidirectional temporal method performs much better and we can clearly observe that it is independent of the last optical flow. In this case the errors are not so stable and its behaviour is very similar to the spatial method. This means

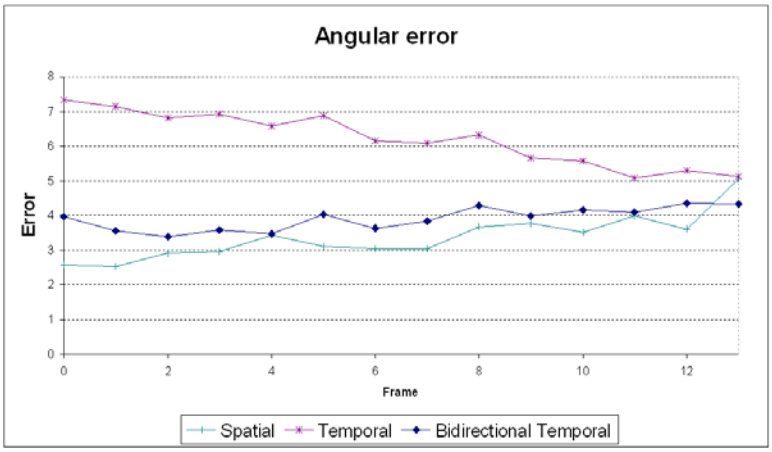

Figure 11: Angular error for the Yosemite sequence.

that the temporal term make worse estimates but in some sense it is reduced by means of the threshold effect of the $\Phi(.)$ function.

Method	AE_μ	AE_σ	EE_μ	EE_σ
Spatial	$3{,}37^o$	$0{,}65^o$	0,19	0,06
Temporal	$6{,}21^o$	$0{,}77^o$	0,35	0,02
Bi-Temporal	$3{,}90^o$	$0{,}33^o$	0,23	0,05

Table 3: Mean angular and euclidean errors for the Yosemite sequence.

In table 3 we show the angular and euclidean errors for this sequence. The standard deviations points out that the stability of the solution is still held in comparison with the spatial solution. The bidirectional temporal method does not diverge of the spatial solution as the simple one does.

A model depending on the temporal derivative of the optical flow – like that proposed in [8] – is more suitable to these kind of displacements because the optical flow is continuous.

5.4 Taxi

For the last test we used the Taxi sequence – Fig. 12 – which is a real sequence that contains 40 frames. This sequence is copyright by H.-H. Nagel (KOGS/IAKS, University of Karlsruhe, Germany, at *http://i21www.ira.uka.de/ image_sequences/*).

In Fig. 13 we show the solutions of the spatial and bidirectional temporal methods.

In this sequence there are four objects that are moving: the car on the left bottom corner, the taxi, the truck on the right bottom corner and a pedestrian on the pavement. The main differences between the spatial and temporal methods are the following: The background in the temporal solution is more stable. The solution for the taxi and the truck are very similar in both cases, but the car seems to be better estimated in the spatial method.

Figure 12: Frames 0, 10 and 19 of the Taxi sequence.

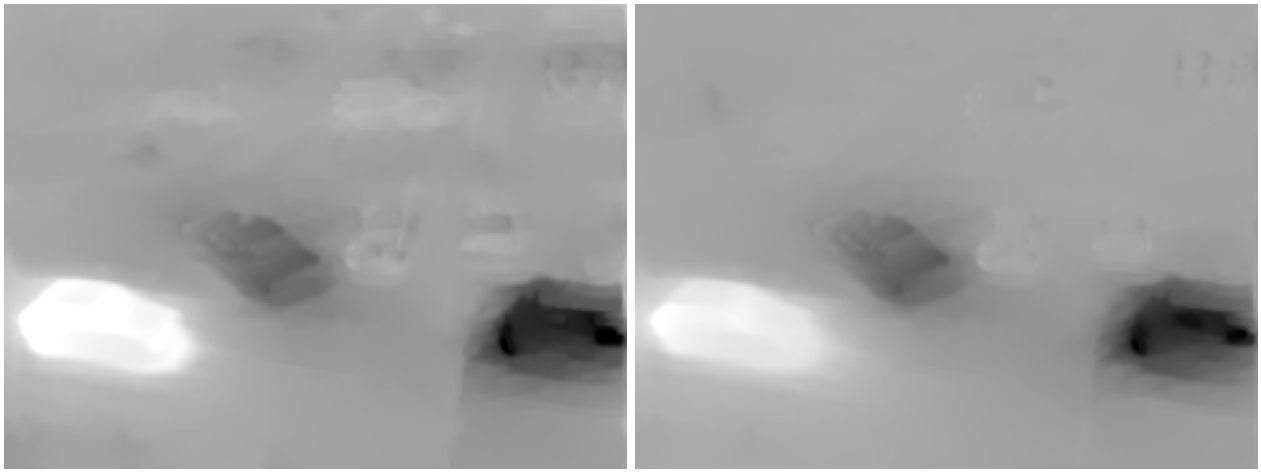

Figure 13: On the left the result of the spatial method; and, on the right, the disparity map obtained with the bidirectional temporal method.

Finally the pedestrian movement appears on the temporal and not on the spatial solution. The most remarkable difference is the background in where the objects are not moving. The spatial regularization is not enough to overcome the problems of local noise and the temporal regularization clearly copes with these small variations.

6 Conclusions

With this work we have proposed a novel variational method that includes a temporal smoothness term. This method may be considered as a generalization of previous related spatial methods. We have overcome the inconveniences of other methods that use a coupled temporal–spatial regularizing term which is more suitable for small displacements due to the inclusion of temporal derivatives.

We have created a new term that minimizes the difference of the optical flows that permits large displacements of the objects.

There are some authors that claim that the temporal and spatial regularizations should be treated in the same manner. This is true if we assume the continuous model. Once we have assumed a discontinuous model then it is not convenient to model the temporal and spatial regularizers in the same way.

The design of this new term promotes the constant velocity of particles all through the

sequence, so it is well suited for sequences that are translating in a fixed direction. There will not be any improvement for non translating motions, but due to the $\Phi(.)$ function in the temporal smoothness term there will be a small penalisation if other kind of displacements are present.

We have shown the necessity of including the backward flow in the energy functional. All the comparisons show that the bidirectional temporal method clearly outperforms the simpler temporal method.

As we can observe in the experimental results, the numerical studies show that this method provides more stable results. We have also shown that when translating motions are present on the scene then there is an increase of accuracy in all the frames.

To our knowledge, this is the first approach that considers temporal regularizations with large displacements. It is specially good for translational movements and it does not get far solutions from the spatial method if other displacements are present.

In future works we will examine more general temporal smoothnes terms that allow us to consider different kind of displacements. It seems natural to use the temporal information to try to improve the optical flow, but there is still a lot of things to understand before finding a basic method that takes into account all the complexity of the temporal dimension.

7 Acknowlegments

The authors would like to thank Joachim Weickert for valuable comments on this work. This work has been partly supported by the spanish research project TIC2003-08957 (MCYT).

A Computing the backward flow, $\mathbf{h}^*$

In this apendix we examine how to compute the backward flow directly from the forward flow. It is easy to see that the correspondence between both flows is

$$\mathbf{h}(\mathbf{x}) = -\mathbf{h}^*(\mathbf{x} + \mathbf{h}(\mathbf{x})) \tag{18}$$

The main difficulty here is to deal with discrete images. In our problem the function $\mathbf{h}(\mathbf{x})$ is real but the locations $\mathbf{x}$ are integers –image pixels–. The $\mathbf{h}^*(\mathbf{x})$ only has values in some discrete positions. As we can see in Fig. 14 the correspondence will not be exact so we have to adjust the value of $\mathbf{h}^*(\mathbf{x})$ depending on the portion of pixels that arrive to our destiny pixel. In general, there will be several correspondences that distruibute their values on a single pixel, so we have to compute an average of all the portions of the flows that fall down in each pixel.

Considering the discrete nature of $\mathbf{h}^*(\mathbf{x})$ we may compute its value in each position according to this functional

$$\mathbf{h}^*(\mathbf{x}_i) = -\frac{\sum_{j=1}^{N} \mathbf{h}(\mathbf{x}_j) p_{i,j}\left(\mathbf{x}_i, \mathbf{x}_j + \mathbf{h}(\mathbf{x}_j)\right)}{\sum_{j=1}^{N} p_{i,j}\left(\mathbf{x}_i, \mathbf{x}_j + \mathbf{h}(\mathbf{x}_j)\right)}$$

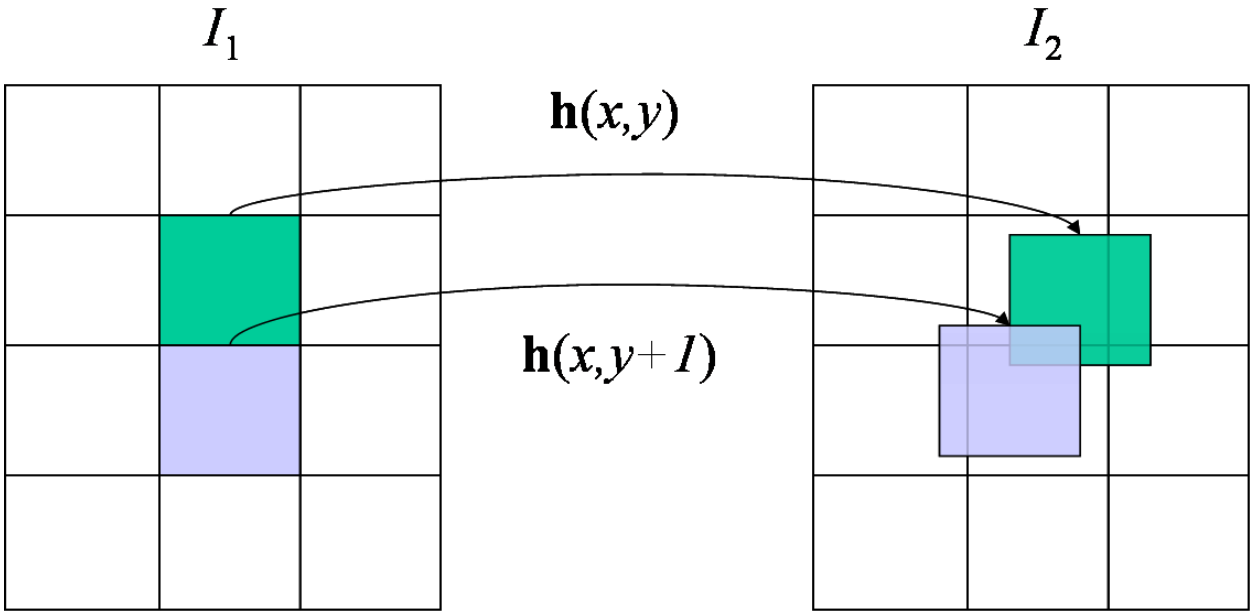

Figure 14: The composition of an integer position, $\mathbf{x}$, and the real function, $\mathbf{h}(\mathbf{x})$, generate a mismatching in the positions of $\mathbf{h}^*(\mathbf{x})$. As we can see in this figure, we have to divide each correspondence in four different estimates –four different pixels– in order to compute the values of the discrete function $\mathbf{h}^*(\mathbf{x})$.

where N is the size of the image and $p_{i,j}$ stands for the area of the pixel that is covered by the optical flow as can be seen in Fig. 14. Each $\mathbf{x}_j+\mathbf{h}(\mathbf{x}_j)$ will generate four different $p_{i,j}$ that will lie on neighouring pixels. Lets see how we compute these weights. To simplify we call $\mathbf{a} = (a_x, a_y) = \mathbf{x}_i$ and $\mathbf{b} = (b_x, b_y) = \mathbf{x}_j+\mathbf{h}(\mathbf{x}_j)$

$$p_{i,j}(\mathbf{a},\mathbf{b}) = \begin{cases} (1-(b_x-a_x))\cdot(1-(b_y-a_y)) & if\ a_x < b_x\ and\ a_y < b_y \\ (1-(b_x-a_x))\cdot(b_y-a_y) & if\ a_x < b_x\ and\ a_y > b_y \\ (b_x-a_x)\cdot(1-(b_y-a_y)) & if\ a_x > b_x\ and\ a_y < b_y \\ (b_x-a_x)\cdot(b_y-a_y) & if\ a_x > b_x\ and\ a_y > b_y \\ 0 & if\ distance(\mathbf{a},\mathbf{b}) \geq 1 \end{cases}$$

This is no more than the computation of the proportional area for the four neighbours.

There still remains to consider a further issue which are the empty pixels,$\mathbf{x}_i$, that have no correspondence in the other image –maybe due to occlusions–. Normally these pixels are situated close to the object boundaries in the sense of their displacements.

One way to manage this is to label the pixels as occlusions and to modify the method in order to avoid estimating the flow at these locations or only to apply the regularizing term to the occlusions. This could be a better approach but there are two inconveniences: 1) The first is that we only detect these occlusions in $\mathbf{h}^*(\mathbf{x}_i)$ so we would favour one of the estimates; 2) The second is that handling occlusions is not straight forward and there is an overload on the formulation of the method. Our purpose here is not to propose a complex method but

only to study the behaviour of temporal smoothness terms. In papers [2] and [1] we have presented two works on the estimation of symmetrical optical flows for two images in where we dealt with occlusions.

For these reasons we apply a post–processing step in order to fill up the holes. This is a simple step in where after several iterations we complete the information of the holes by averaging with the information from the neighbours.

References

[1] L. Alvarez, R. Deriche, T. Papadopoulo and J. Sánchez, Symmetrical dense optical flow estimation with oclussions detection. International Journal of Computer Vision. Preprint, 2006.

[2] L. Alvarez, R. Deriche, T. Papadopoulo and J. Sánchez, Symmetrical dense optical flow estimation with oclussions detection. ECCV 2002, Lecture Notes in Computer Science, Vol. 1, pp. 721–735, 2002.

[3] L. Alvarez, J. Weickert, and J. Sánchez, Reliable Estimation of Dense Optical Flow Fields with Large Displacements. International Journal of Computer Vision, Vol. 39, **1** (2000) 41–56. An extended version maybe be found at Technical Report n^{o}2 del Instituto Universitario de Ciencias y Tecnologías Cibernéticas

[4] P. Anandan, A Computational Framework and an Algorithm for the Measurement of Visual Motion. International Journal of Computer Vision, 2, pp. 283–310, 1989

[5] M. J. Black and P. Anandan, Robust dynamic motion estimation over time. In Proc. 1991 IEEE Computer Society Conference on Computer Vision an d Pattern Recognition, pp 292–302, June 1991

[6] M. J. Black and P. Anandan, Robust Incremental Optical Flow. In Proc. Conference on Computer Vision and Pattern Recognition, pp. 296–302, 1992

[7] M. Black and A. Rangarajan, On the Unification of Line Processes, Outlier Rejection and Robust Statistics with Applications in Early Vision. International Journal of Computer Vision, Vol. 19, pp 75–104, 1996

[8] T. Brox, A. bruhn, N. Papenberg and J. Weickert, High Accuracy Optical Flow Estimation Based on a Theory for Warping. In Proc. 8th European Conference on Computer Vision, Springer LNC 3024, Vol. 4, pp. 25–36, May 2004

[9] I. Cohen, Nonlinear Variational Method for Optical Flow Computation. Proc. of the 8th Scandinavian Conference on Image Analysis, Norway, 1993.

[10] R. Deriche, P. Kornprobst and G. Aubert, Optical flow estimation while preserving its discontinuities: a variational approach. In Proc. Second Asian Conference on Computer Vision, Vol. 2, pp. 290–295, Dec. 1995

[11] W. Enkelmann, Investigation of Multigrid Algorithms for the Estimation of Optical Flow Fields in Image Sequences. Comput. Vis. Graph. Image Process., Vol. 43, pp. 150–177, 1988

[12] H. W. Haussecker and D. J. Fleet, Computing Optical Flow with Physical Models of Brightness Variations. IEEE Transactions on Pattern Analysis and Machine Intelligence, 23(6), June 2001

[13] G. Hermosillo, C. Chefd'Hotel and O. Faugeras, Variational Methods for Multimodal Image Matching. International Journal of Computer Vision, 50(3), pp. 329–343, 2002

[14] B. Horn and B. Schunck: Determining Optical Flow. Artificial Intelligence, Vol. 17, pp.185–203, 1981

[15] E. Mémin and P. Pérez, Dense Estimation and Object–Based Segmentation of the Optical Flow with Robust Techniques. IEEE Transactions on Image Processing, 7(5), pp. 703–719, 1998

[16] E. Mémin and P. Pérez, Hierarchical estimation and segmentation of dense motion fields. International Journal of Computer Vision, 46(2), pp. 129–155, 2002

[17] H. H. Nagel, Extending the 'oriented smoothness constraint' into the temporal domain and the estimation of derivatives of optical flow. ECCV 90, Lecture Notes in Computer Science, Vol. 427, pp. 139–148, 1990

[18] H. H. Nagel and W. Enkelmann: An Investigation of Smoothness Constraints for the Estimation of Displacements Vector Fields from Image Sequences. IEEE Trans. Pattern Anal. Mach. Intell. 8, 565–593, 1986

[19] P. Perona and J. Malik: Scale-Space and Edge Detection Using Anisotropic Diffusion. IEEE Transactions on Pattern Analysis and Machine Intelligence **12** (1990) 429–439

[20] M. Proesmans, L. Van Gool and A. Oosterlinck, Determination of optical flow and its discontinuities using non-linear diffusion, Proc. ECCV'94, pp. 295-304, 1994

[21] P. Viola and W. M. Wells, Alignment by Maximization of Mutual Information. International Journal of Computer Vision, Vol. 24, pp. 137–154, 1997

[22] W. M. Wells, P. Viola, H. Atsumi, S. Nakajima and R. Kinikis, Multimodal Volume Registration by Maximization of Mutual Information. Medical Image Analysis, Vol. 1, pp. 35–51, 1996

[23] J. Weickert and C. Schnörr: Variational Optic Flow Computation with a Spatio–Temporal Smoothness Constraint. Journal of Mathematical Imaging and Vision **14**, pp. 245–255, 2001

[24] J. Weickert and C. Schnörr: A Theoretical Framework for Convex Regularizers in PDE-Based Computation of Image Motion. International Journal of Computer Vision, 45(3), pp. 245–264, 2001

Instituto Universitario de Ciencias y Tecnologías Cibernéticas
Universidad de Las Palmas de Gran Canaria
Campus de Tafira
35017 Las Palmas, España
http://www.iuctc.ulpgc.es